

End Point Detection of Fillet Weld Using Mechanized Rotating Arc Sensor in GMAW

A sensing model was developed to detect the end points of joints in fillet welds using gas metal arc welding with a rotating arc

BY W.-S. YOO, Y.-H. SHI, J.-T. KIM, AND S.-J. NA

KEYWORDS

Gas Metal Arc Welding (GMAW)
Rotating Arc Sensor
Contact Tip-to-Work Distance
Fillet Welds

ABSTRACT. In this paper, a geometrical sensing model was developed for the rotating arc sensor in gas metal arc welding (GMAW) of fillet joints that have open and closed ends, considering the mathematical model of the GMA welding system. By using the two developed models, simulations of welding current of the rotating arc sensor were performed and compared with the experimental results of current waveform in open and closed fillet joints in steel welding.

Introduction

Through-arc sensing using the electric signals obtained from the welding arc is the most effective way to track the weld joint. During gas metal arc welding (GMAW) with a constant voltage power source, the welding current and the voltage generally vary with the contact tip-to-work distance (CTWD) (Ref. 1). The gun weaving method is widely used to intentionally stimulate the variations of the CTWD. But the conventional gun weaving methods have a relatively poor resolution and limit the oscillation frequency due to the mechanical restraints. To overcome these shortcomings, the arc sensing systems enhanced using the mechanical arc rotation or the electromagnetic arc oscillation have been investigated and successfully developed (Refs. 2, 3).

The rotating arc sensor can improve the sensor characteristics such as the sensitivity and the responsiveness due to the high-speed rotation frequency. During high-speed rotating arc welding, self-regulation of the welding arc is not fully performed because the period of rotation is shorter than the time constant of the self-regulation process (Ref. 1). The rapid change in CTWD generates the variation in the arc length rather than in the electrode extension length. Therefore, the rotating arc sensor operates in a dynamic state enhancing its sensitivity (Ref. 4). This insufficient self-regulation enables development of the arc sensor for aluminum alloy welding for which it is known that the application of the weaving arc sensor is limited (Ref. 5). Moreover, the rotating arc can increase the responsiveness, which is inherently related to the oscillation frequency.

In addition to joint tracking, through-arc sensing can be ap-

plied to detecting the end point of the weld joint because the shape of the joint is reflected on the electrical signals such as welding current and voltage, which are related to the CTWD. Rotating arc welding has two prominent features in detecting the end point: One is that the effect of weld pool can be reduced when the arc rotates along the front half-circular path. The other is that its enhanced responsiveness ensures the rapid detection of an end point.

In this paper, the following topics are investigated: a) A mathematical model that investigates the GMA welding system; b) a geometrical sensing model of the rotating arc sensor in fillet welding that has open and closed ends; and c) current simulations and experiments in open and closed fillet structures in steel welding.

Mathematical Model of GMA Welding System

Figure 1 shows the equivalent electrical circuit of the conventional GMA welding system with a constant voltage power source. In the equivalent electrical circuit, the output voltage of the welding power source, V_s , and the voltage drop in the welding power cable, V_p , can be written as follows:

$$V_s = V_{oc} - R_s I - L_s \frac{dI}{dt} \quad (1)$$

$$V_p = R_p I + L_p \frac{dI}{dt} \quad (2)$$

The voltage drop in the welding arc, V_a , can be written as follows:

$$V_a = V_{ao} + R_a I + E_a L_a \quad (3)$$

where V_{oc} is the internal voltage of the welding power source; R_s is the internal electrical resistance of the welding power source; L_s is the internal inductance of the welding power source; V_p , R_p , and L_p are the voltage drop, the resistance, and the inductance of the welding cable, respectively; V_{ao} is the constant in the welding model; and R_a , L_a , and E_a are the resistance, the length, and the electric field of the arc, respectively.

For the modeling of the GMA welding system, many researchers investigated the welding wire melting phenomenon at the end. Lesnewich (Ref. 6) investigated the relation between the wire melting rate, the wire extension length, and the welding current experimentally. Halmoy (Ref. 5) induced the same relation in the static state that the welding wire feeding and melting rate are equivalent. Mao and Ushio (Ref. 4), and Shepard and Cook (Ref. 7) introduced the idea of action integral. They integrated the square of the welding current during the time that the welding wire moves from the gun tip to the molten pool. Zhu et al. (Ref. 8) investigated the welding wire melting phenomenon by the transient temperature analysis model. Kim (Ref. 9) presented the dy-

W.-S. YOO is with LS Cable Ltd., Production Engineering Center, Gyeonggi-do, Korea. Y.-H. SHI is with South China University of Technology, School of Mechanical Engineering, Guangzhou, China. J.-T. KIM and S.-J. NA are with Korea Advanced Institute of Science and Technology, Department of Mechanical Engineering, Daejeon, Korea.

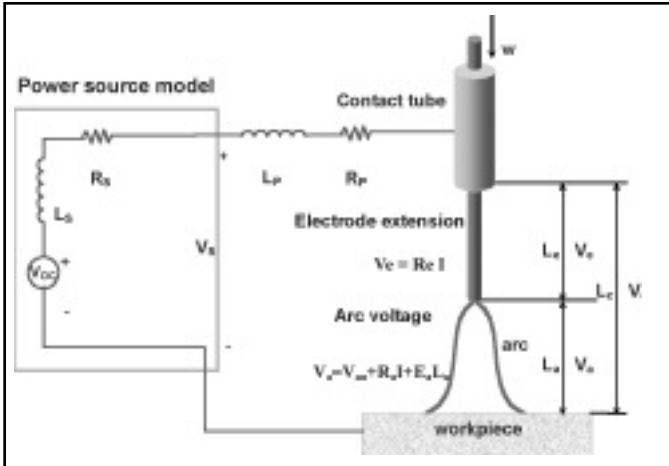


Fig. 1 — Equivalent circuit of GMA welding system using CV power source.

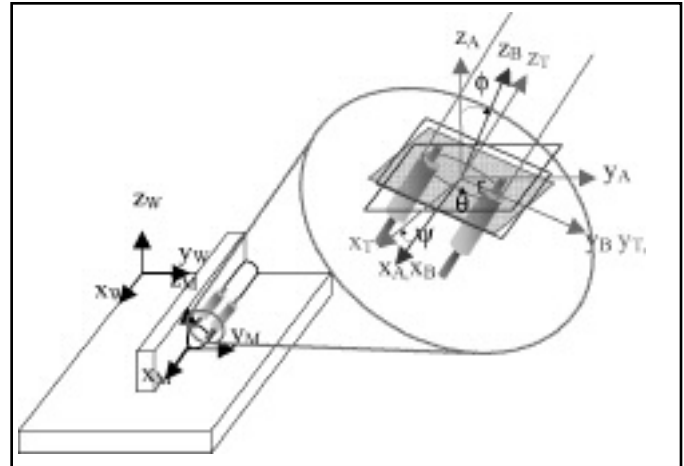


Fig. 2 — Definition of coordinate systems for simulation.

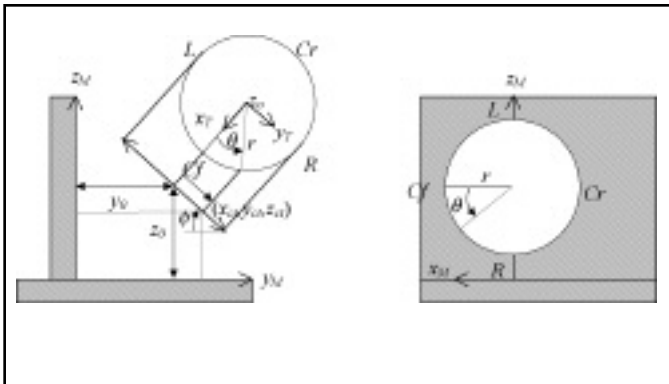


Fig. 3 — Dimensional parameters for welding wire extension end position.

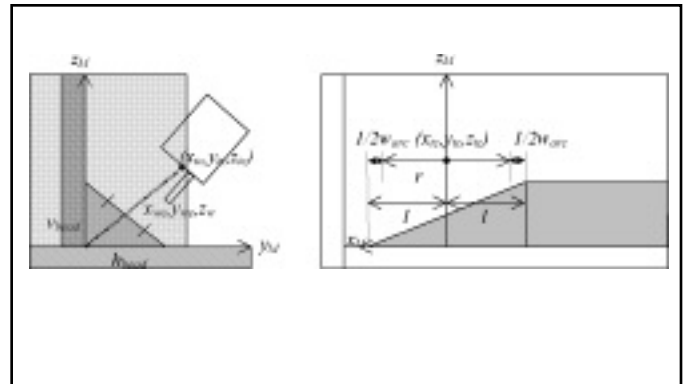


Fig. 4 — Bead model in fillet welding.

dynamic simulation of welding wire melting by using the variable space network method and by modeling the heat flux from the molten end of the welding wire into the electrode.

In Halmoy's (Ref. 5) melting model, the voltage drop at the welding wire extension (V_e) is written as follows:

$$V_e = \frac{v_f S}{I} H_e = \frac{a L_e I}{S} - \frac{b v_f S}{I} \quad (4)$$

where a is the resistance at the welding wire extension; b is the thermal energy of welding wire at room temperature; L_e is the welding wire extension; v_f is the welding wire feed rate; and S is the welding wire cross-sectional area.

In Equation 4, Joule heat at welding wire tip, H_e , is written as follows:

$$H_e = \frac{a L_e I^2}{S^2 v_f} - b \quad (5)$$

The quantity of heat from the arc at welding wire tip, H_a , is written as follows:

$$H_a = \frac{\Phi I}{v_m S} \quad (6)$$

where Φ is the equivalent arc voltage for wire melting phenome-

non and v_m is wire melting speed.

If the quantity of heat necessary to heat the welding wire to melting temperature is denoted by H_o , the following equation is established from the energy conservation rule.

$$H_o = H_e + H_a \quad (7)$$

The equation of the melting characteristics can be obtained from Equations 5–7, as follows:

$$v_m = \frac{A I}{1 - B \left(L_e / v_f \right) I^2} \quad (8)$$

where, $A = \frac{\Phi}{S(H_o + b)}$ and $B = \frac{a}{S^2(H_o + b)}$.

The welding wire extension length, L_e , can be obtained from Equation 8 as follows:

$$\frac{dL_e}{dt} = v_f - v_m = v_f - \frac{A I}{1 - B \left(L_e / v_f \right) I^2} \quad (9)$$

Through simultaneous solution of Equations 1–4, it is possible

to determine the variation in welding current depending on the wire extension and arc length as follows:

$$\frac{dI}{dt} = \frac{V_{oc} - V_{a0}}{L_s + L_p} - \frac{R_s + R_p + R_a + \frac{aL_e}{S}}{L_s + L_p} I + \frac{bSv_f}{(L_s + L_p)I} - \frac{E_a}{L_s + L_p} L_a \quad (10)$$

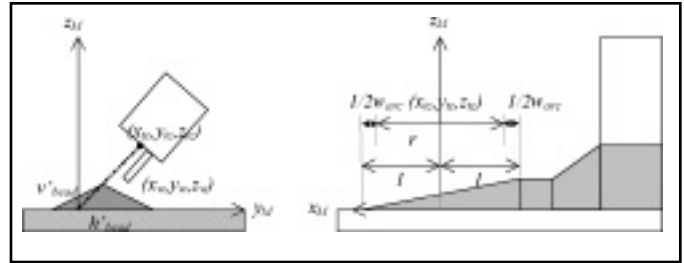


Fig. 5 — Bead model after fillet end in open fillet welding.

Geometrical Model of Fillet Welding

To simulate the waveform of welding current during actual fillet welding, geometrical models of fillet welding are developed. Figure 2 shows the target weld geometry and the definition of coordinate systems. W is the frame fixed to the weld structure and M is the frame moving along to the weld joint, while A is the frame moving with the gun. The origin of A is defined as the center of the rotating gun tip. The frames W, M, and A have the same direction cosine, but different origins. B is the frame moving with the same origin of A and rotated by the angle of Φ with respect to the axis x of A. T is the frame moving with the same origin as A and rotated by the angle of ψ with respect to the axis y of B.

Transformation matrices between frames defined in Fig. 2 are determined as follows:

$${}^W_M T = \begin{bmatrix} 1 & 0 & 0 & v_{welding} t \\ 0 & 1 & 0 & y_{offset} \\ 0 & 0 & 1 & 0 \\ 0 & 0 & 0 & 1 \end{bmatrix} \quad (11)$$

$${}^M_A T = \begin{bmatrix} 1 & 0 & 0 & 0 \\ 0 & 1 & 0 & y_0 \\ 0 & 0 & 1 & z_0 \\ 0 & 0 & 0 & 1 \end{bmatrix} \quad (12)$$

$${}^A_B T = R_X(\phi) = \begin{bmatrix} 1 & 0 & 0 & 0 \\ 0 & \cos \phi & -\sin \phi & 0 \\ 0 & \sin \phi & \cos \phi & 0 \\ 0 & 0 & 0 & 1 \end{bmatrix} \quad (13)$$

$${}^B_T T = R_Y(\psi) = \begin{bmatrix} \cos \psi & 0 & \sin \psi & 0 \\ 0 & 1 & 0 & 0 \\ -\sin \psi & 0 & \cos \psi & 0 \\ 0 & 0 & 0 & 1 \end{bmatrix} \quad (14)$$

where $v_{welding}$ is the welding speed; t is the time elapsed; and y_{offset} is the distance of the joint along the y axis of the frame W. (y_0, z_0) is the coordinate point of the origin of A referenced to the frame M. Figure 3 shows the dimensional parameters needed to determine the welding wire end position.

The coordinate point of the welding wire end position, p_{we} , with respect to the frame T can be expressed as follows:

$${}^T p_{we} = \begin{bmatrix} r \cos \theta \\ r \sin \theta \\ -L_e \\ 1 \end{bmatrix} \quad (15)$$

where r is the rotation radius and θ is the rotating angle of the gun with respect to the frame T.

Rotating speed of the gun can be obtained by the rotating frequency, f_r , as follows:

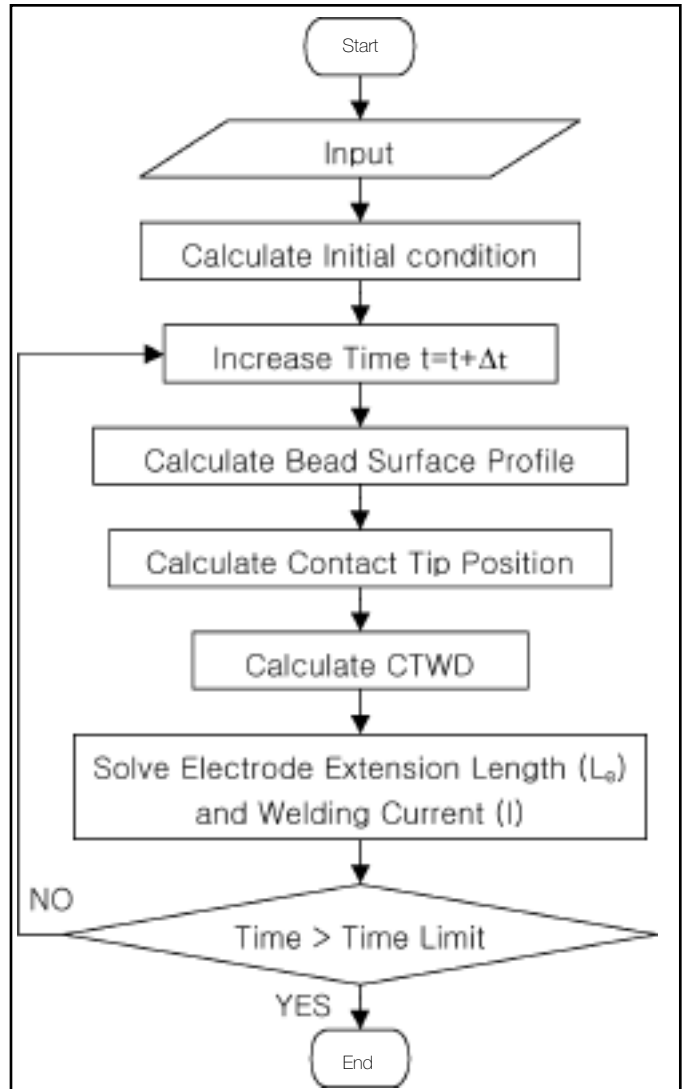


Fig. 6 — Flow chart for calculation of electrode extension length and welding current.

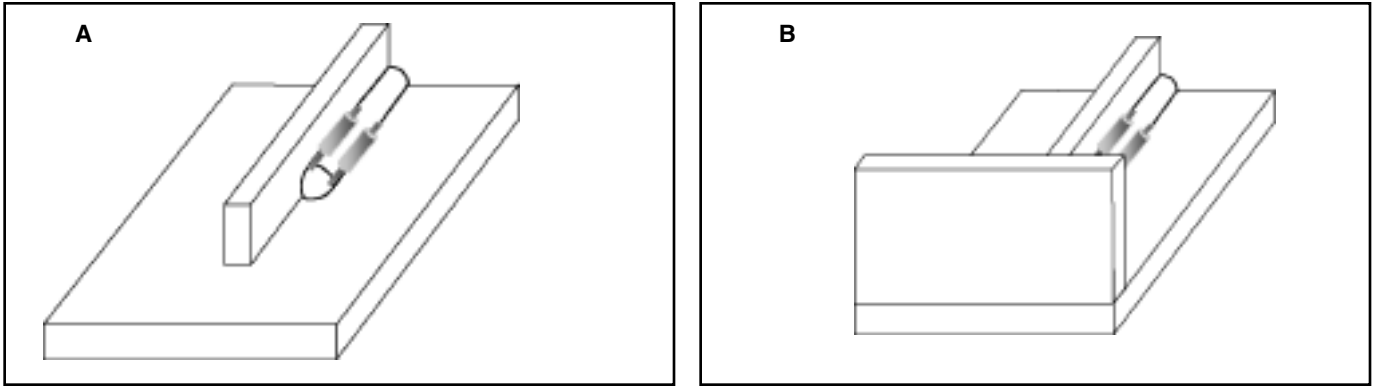


Fig. 7 — Weld structures for simulation. A — Open fillet joint welding; B — closed fillet joint welding.

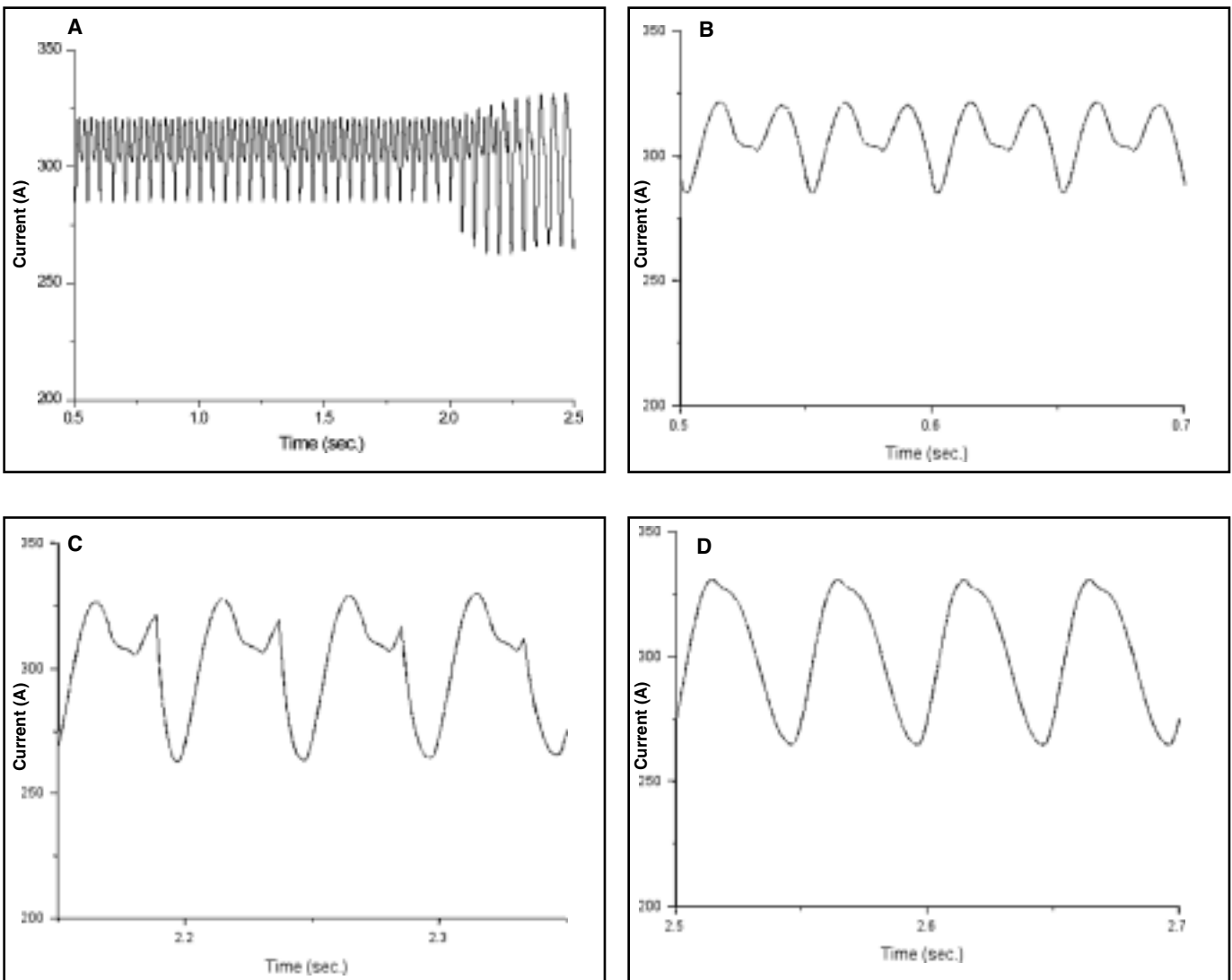


Fig. 8 — Simulation results (open structure, $\phi = -45$ deg, $\psi = 0$ deg). A — Simulated waveform of welding current; B — fillet joint region; C — transition region; D — after end point.

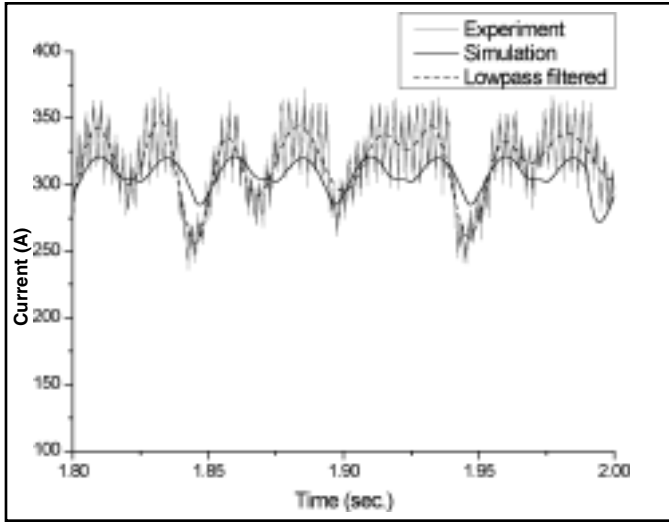


Fig. 9 — Simulated and experimental welding current waveform in fillet joint region of open structure ($\phi = -45$ deg, $\psi = 0$ deg).

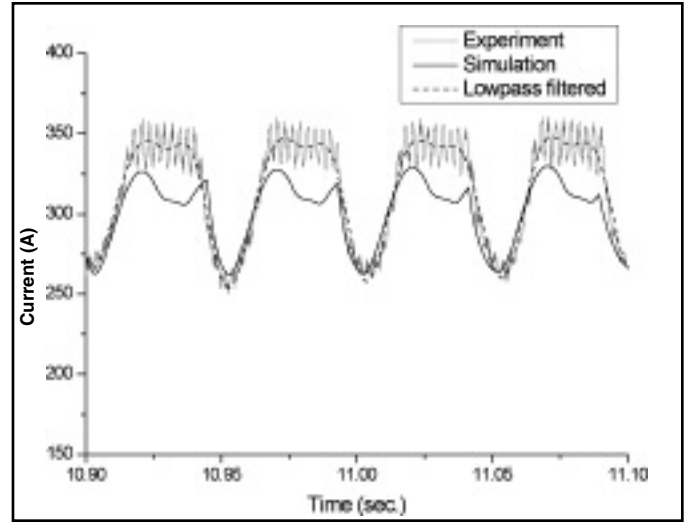


Fig. 10 — Simulated and experimental welding current waveform in transition region of open structure ($\phi = -45$ deg, $\psi = 0$ deg).

$$\frac{d\theta}{dt} = 2\pi f_r \quad (16)$$

The coordinate point of the welding wire end position with respect to W can be obtained from the previous equations as follows:

$${}^W P_{we} = \begin{bmatrix} r \cos \theta \cos \psi - L_e \sin \psi + v_{welding} t \\ r \sin \theta \cos \phi + r \cos \theta \sin \phi \sin \psi + L_e \sin \phi \cos \psi + y_o + y_{offset} \\ r \sin \theta \sin \phi - r \cos \theta \cos \phi \sin \psi - L_e \cos \phi \cos \psi + z_o \\ 1 \end{bmatrix} \quad (17)$$

It is necessary to know the bead geometry to simulate the welding current from the previous equations. To model the weld bead shape, the following two conditions were assumed:

- 1) Volume of the welding wire fed equals the volume of the bead formed
- 2) Cross-sectional view of the bead is triangular.

After the welding gun was passed, the cross-sectional view of the bead from the x direction was approximated as a right-angle triangle. When the bead is forming under the rotating arc gun, the cross-sectional area of the bead from the x direction was approximated as linearly decreasing along the direction the gun was moving. Figure 4 shows the bead shape modeled in the joint of the fillet weld. The relations between welding conditions and bead parameters are established as follows:

$$\frac{1}{4} \pi d_w^2 v_f = \frac{1}{2} v_{bead} h_{bead} v_{welding} \quad (18)$$

where d_w is the diameter of the welding wire; v_f is the wire feed rate; $v_{welding}$ is the welding speed; and v_{bead} and h_{bead} are, respectively, the leg length in the vertical direction and in the horizon direction. If the line between the origin of frame M and the origin of frame T pass through the mid-point of the bead surface's projected line, Equation 19 can be obtained.

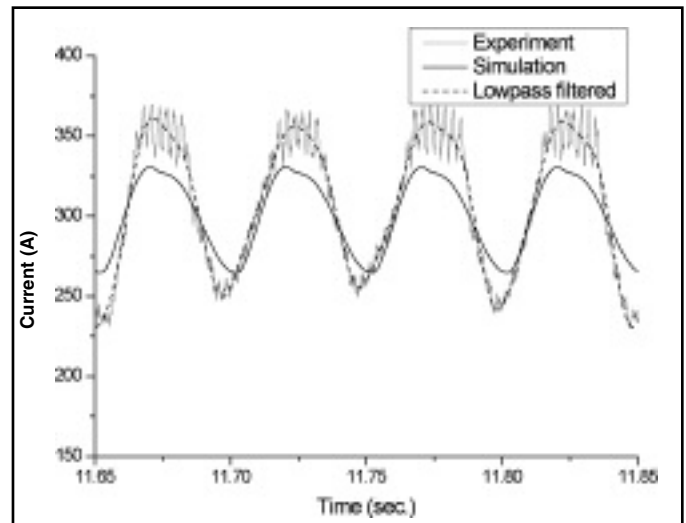


Fig. 11 — Simulated and experimental welding current waveform after the end of the fillet joint region of open structure ($\phi = -45$ deg, $\psi = 0$ deg).

$$M z_{ic} = \frac{v_{bead}}{h_{bead}} M y_{ic} \quad (19)$$

where, ($M z_{ic}, M y_{ic}$) is the coordinate value of the origin of frame T with respect to frame M.

Horizontal and vertical leg length can be calculated from Equations 18 and 19 as follows:

$$h_{bead} = \sqrt{\frac{\pi d_w^2 v_f M y_{ic}}{2 v_w M z_{ic}}} \quad (20)$$

$$v_{bead} = \sqrt{\frac{\pi d_w^2 v_f M z_{ic}}{2 v_w M y_{ic}}} \quad (21)$$

The surface equation of the bead with respect to frame M can be obtained as follows:

$$\frac{1}{l} M_x + \frac{2}{h_{bead}} M_y + \frac{2}{v_{bead}} M_z - 1 = 0 \quad (22)$$

If the arc is generated in the shortest way from the tip to bead or workpiece, the arc length during fillet joint welding can be obtained as follows:

$$L_a = \min \left(\begin{array}{l} W_{x_{end}} - W_{x_w}, M_{y_w}, M_{z_w}, \\ \frac{1}{l} M_x + \frac{2}{h_{bead}} M_y + \frac{2}{v_{bead}} M_z - 1 \\ \sqrt{\left(\frac{1}{l}\right)^2 + \left(\frac{2}{h_{bead}}\right)^2 + \left(\frac{2}{v_{bead}}\right)^2} \end{array} \right) \quad (23)$$

where, $(W_{x_w}, W_{y_w}, W_{z_w})$ is the coordinate value of the end of the welding wire with respect to W; and $W_{x_{end}}$ is the coordinate value of the end of the joint with respect to W in closed fillet welding.

After the fillet end, bead-on-plate welding with inclined rotating arc forms the bead shape as shown in Fig. 5. If the horizontal and vertical leg lengths are assumed as in Equations 24 and 25, the equation of bead surface near the gun tip is obtained as Equation 26.

$$h'_{bead} = 2 h_{bead} \quad (24)$$

$$v'_{bead} = \frac{1}{2} v_{bead} \quad (25)$$

$$\begin{aligned} & \frac{h'_{bead}}{4l} \left(\frac{M_{y_{tc}}}{M_{z_{tc}}} v'_{bead} + \frac{h'_{bead}}{4} \right) x + \frac{1}{4l} \left(\frac{M_{y_{tc}}}{M_{z_{tc}}} v'_{bead} + \frac{h'_{bead}}{4} \right) y \\ & + \frac{1}{2 \frac{v'_{bead}}{h'_{bead}}} \left(\frac{M_{y_{tc}}}{M_{z_{tc}}} v'_{bead} + \frac{h'_{bead}}{4} \right) z - 1 = 0 \end{aligned} \quad (26)$$

The arc length after the fillet end can be obtained as follows:

$$L_a = \min \left(\begin{array}{l} M_{y_w}, M_{z_w}, \\ \frac{h'_{bead}}{4l} \left(\frac{M_{y_{tc}}}{M_{z_{tc}}} v'_{bead} + \frac{h'_{bead}}{4} \right) M_{x_w} + \frac{1}{4l} \left(\frac{M_{y_{tc}}}{M_{z_{tc}}} v'_{bead} + \frac{h'_{bead}}{4} \right) M_{y_w} + \frac{1}{2 \frac{v'_{bead}}{h'_{bead}}} \left(\frac{M_{y_{tc}}}{M_{z_{tc}}} v'_{bead} + \frac{h'_{bead}}{4} \right) M_{z_w} - 1 \\ \sqrt{\left(\frac{h'_{bead}}{4l} \left(\frac{M_{y_{tc}}}{M_{z_{tc}}} v'_{bead} + \frac{h'_{bead}}{4} \right) \right)^2 + \left(\frac{1}{4l} \left(\frac{M_{y_{tc}}}{M_{z_{tc}}} v'_{bead} + \frac{h'_{bead}}{4} \right) \right)^2 + \left(\frac{1}{2 \frac{v'_{bead}}{h'_{bead}}} \left(\frac{M_{y_{tc}}}{M_{z_{tc}}} v'_{bead} + \frac{h'_{bead}}{4} \right) \right)^2} \end{array} \right) \quad (27)$$

Simulation Results and Discussion

The mathematical model of the GMA welding system, the electrode melting model, and the geometrical model of the weld bead were used to simulate the current waveform of the rotating arc. Equations 9, 10, 23, and 27 were calculated simultaneously. To solve the differential equation, a 4th order Runge-Kutta method was used. Simulations were done as shown in Fig. 6. Table 1 shows the welding conditions and parameters used in the simulations. Two series of simulations are presented and discussed for two different types of welding end of the fillet joint.

Open Fillet Structure

Figure 7A shows the open fillet structure adopted for simulations, and simulation results of welding current waveform for this structure are shown in Fig. 8. Before approaching the fillet end, the welding current fluctuates twice during a cycle of arc rotation. After passing the fillet end, however, the welding current fluctuates only once during a cycle of arc rotation. The variation of arc length due to the arc rotating, the bead geometry, and fillet joint geometry with an open end probably cause the different fluctuations of the simulated welding current. To validate the simulation results, comparisons between the current waveform of the simulations and that of the experiments were performed in Figs. 9–11. The current waveform measured in rotating arc welding shows a higher frequency than the simulated one or low-pass filtered one. This multiple of 60 Hz is due to the three-phase 60-Hz power frequency of the SCR supply. The overall frequency of the current waveform is 40 Hz in fillet joint region, but decreases in the transition region, and finally reaches 20 Hz after end of the fillet joint, which is the frequency of gun rotation. All the comparisons show that the simulation results are well suited to the experiments. Table 2 shows the welding conditions used in welding experiments.

Closed Fillet Structure

Figure 7B shows the closed fillet structure adopted for simulations, and simulation results of the current waveform for this structure are shown in Fig. 12. Before approaching the fillet end, the welding current fluctuates twice during each cycle of arc rotation, which is the same as it does in the open fillet structure (as shown in Fig. 9). Approaching the fillet end, however, the welding current tends to fluctuate three times during each cycle of arc rotation. The reason for these different current waveforms is due to the varia-

Table 1 — Welding Conditions and Parameters for Simulations

Welding Parameters	Welding current (I_0)	280 A
	Welding wire feed rate (v_f)	135 mm/s
	Contact tip to work distance (CTWD)	15 mm
	Welding speed ($v_{welding}$)	6 mm/s
	Rotation diameter	2 mm
Welding Machine Parameters	Inductance ($L_s + L_p$)	0.00018 H
	Resistance ($R_s + R_p$)	0.008 Ω
	Rotating frequency (f_r)	20 Hz
	Source voltage (V_{Oc})	35 V
Arc Parameters	Electric field parameter (E_a)	2.0 V/mm
	Resistance (R_a)	30.7 m Ω
	Arc diameter (w_{arc})	5 mm
Shielding Gas Parameter (CO_2)	Arc voltage (V_a)	15.22 V
	Specific heat ($H_o = H_a + H_c$)	11.1 J/mm ³
Welding Wire	Equivalent voltage (Φ)	3.48 V
	Diameter (D_w)	1.2 mm
	Resistance length (a)	1.2 x 10 ⁻³ Ω mm
	Thermal energy (b)	3.98 J/mm ³

Table 2 — Welding Conditions for Experiments

Welding Machine	600 A, SCR
Welding Wire	DW100 1.2-mm wire
Shielding Gas	CO ₂ 20 L/min
Gun Angle	45 deg
CTWD	15 mm
Rotation Diameter	2 mm
Base Metal, Stiffener	12-mm thick, mild steel

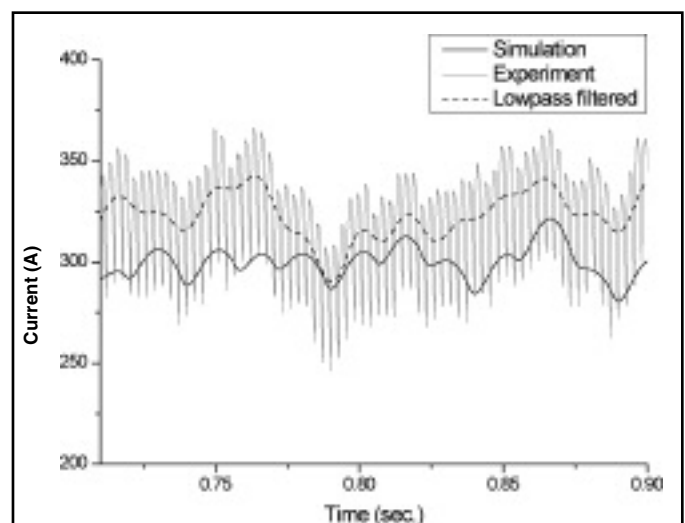
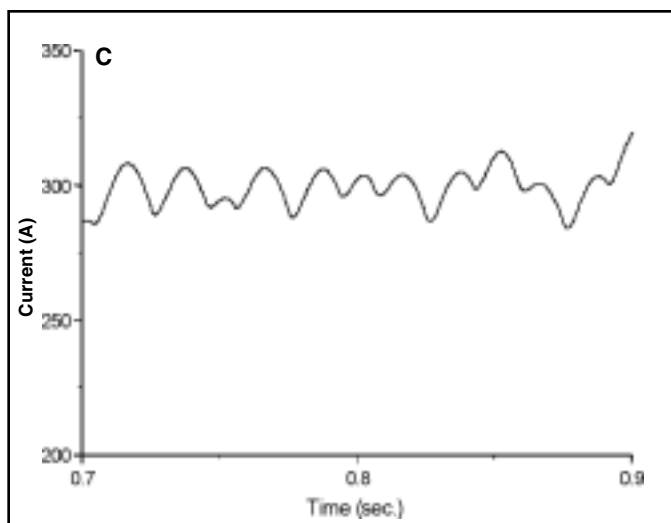
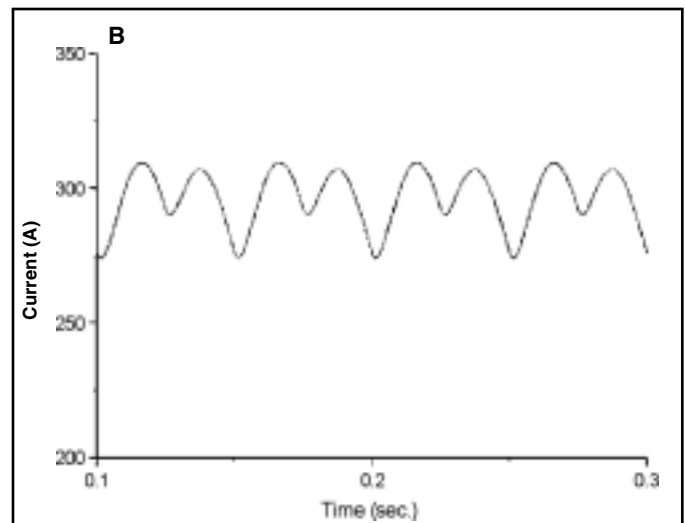
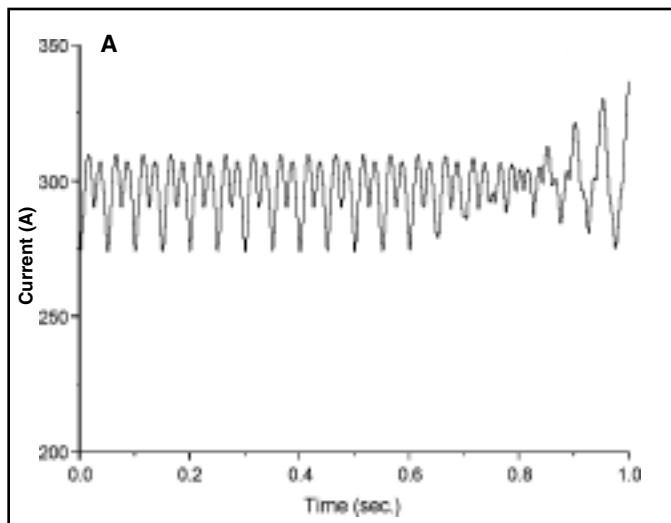


Fig. 12 — Simulation results (closed structure, $\phi = -45$ deg, $\psi = -15$ deg). A — Simulated waveform of welding current; B — fillet joint region; C — in front of the end plate.

Fig. 13 — Simulated and experimental welding current waveform at the end of the fillet joint of closed structure ($\phi = -45$ deg, $\psi = -15$ deg).

tions of arc length during arc rotation, depending on the distance between the welding wire end and the bead geometry or the fillet joint geometry with a vertical end plate. The variation of the current waveform is, however, less distinct than that of the open fillet structure, which cause a difficulty in implementing the algorithm of end point detection of fillet welds for GMAW with a rotating arc. To validate the simulation results, the current waveform of simulations at the fillet end is compared with that of experiments (as shown in Fig. 13). The average current value of the experiment is a little higher than that of the simulation. It is caused by the decrease in the average value of arc length during each rotation cycle, which is due to the abnormal increase in the weld bead height at the end of the closed fillet structure because the vertical end plate blocked the flow of the melted metal. Figure 13 shows that the simulation result and the experimental result are in fairly good agreement with respect to the signal frequency, although very careful measurement will be essential for the application of the end point detection algorithm for a closed fillet structure in GMAW with a rotating arc.

Conclusions

A mathematical sensing model of a rotating arc, which contains the GMA welding system model and the geometrical bead model, was developed. A GMA

welding system model was derived from the equivalent electrical circuit of the conventional welding system with a constant voltage power source and Halmoy's welding wire melting model, which was known to be well suited to experimental results. Geometrical bead models were developed under the simple assumptions for fillet welding with an inclined rotating arc. Welding current simulations were performed by the developed sensing model of the rotating arc and compared to the experimental results in gas metal arc welding of open and closed joints in fillet welds. The comparison results show that the developed sensing model is well suited to the experimental results in steel welding and can be applied for the end point detection of joints in GMAW fillet welds with a rotating arc.

Acknowledgment

This work was supported by the Brain Korea 21 Project of the Ministry of Education and Human Resources Development of the Republic of Korea.

References

1. Cook, G. E. 1983. Robotic arc welding: Research in sensory feedback control. *IEEE Transactions on Industrial Electronics* IE-30 (3): 252-268.
2. Kim, C. H., and Na, S. J. 2001. Development of rotating GMA welding system and its

application to arc sensors. *Proc. 11th International Conf. on Computer Tech. in Welding*, Columbus, Ohio. pp. 47-54.

3. Na, S. J., Kim, C. H., and Kang, Y. H. 2002. Gas metal arc welding with controlled rotating and oscillating arc. 7th Inter-University Research Seminar, Bratislava, Slovakia, June 21, pp. 111-120.

4. Mao, W., and Ushio, M. 1997. Measurement and theoretical investigation of arc sensor sensitivity in dynamic state during gas metal arc welding. *Science and Technology in Welding and Joining* 2(5): 191-198.

5. Halmoy, E. 1980. Wire melting rate, droplet temperature and effective anode melting potential. *Arc Physics and Weld Pool Behavior*, The Welding Institute, Cambridge, U.K. pp. 49-54.

6. Lesnewich, A. 1958. Control of melting rate and metal transfer in gas shielded metal-arc welding. *Welding Journal* 37(8): 343-s to 353-s.

7. Shepard, M. E., and Cook, G. E. 1992. A frequency-domain model of self regulation in gas-metal arc welding. *Conference Proceedings 3rd International Conference on Trends in Welding Research*, Gatlinburg, Tenn. June 1-5, pp. 899-903.

8. Zhu, P., Rados, M., and Simpson, W. W. 1997. Theoretical prediction of the start-up phase will improve weld quality. *Welding Journal* 76(7): 269-s to 274-s.

9. Kim, C. H. 2002. *A Study on Automatic Welding by Using Measurement of GMAW Bead Geometry Using Rotating Arc*. PhD dissertation, Korea Advanced Institute of Science and Technology (KAIST).

CAN WE TALK?

The *Welding Journal* staff encourages an exchange of ideas with you, our readers. If you'd like to ask a question, share an idea or voice an opinion, you can call, write, e-mail or fax. Staff e-mail addresses are listed below, along with a guide to help you interact with the right person.

Publisher/Editor

Andrew Cullison
cullison@aws.org, Extension 249
 Article Submissions

Senior Editor

Mary Ruth Johnsen
mjohnsen@aws.org, Extension 238
 Feature Articles

Associate Editor

Howard Woodward
woodward@aws.org, Extension 244
 Society News
 Personnel

Assistant Editor

Kristin Campbell
kcampbell@aws.org, Extension 257
 New Products
 News of the Industry

Managing Editor

Zaida Chavez
zaida@aws.org, Extension 265
 Design and Production

Advertising Sales Director

Rob Saltzstein
salty@aws.org, Extension 243
 Advertising Sales

Advertising Sales & Promotion Coordinator

Lea Garrigan Badwy
garrigan@aws.org, Extension 220
 Production and Promotion

Advertising Production Manager

Frank Wilson
fwilson@aws.org, Extension 465
 Advertising Production

Peer Review Coordinator

Erin Adams
eadams@aws.org, Extension 275
 Peer Review of Research Papers

Welding Journal Dept.
 550 N.W. LeJeune Rd.
 Miami, FL 33126
 (800) 443-9353
 FAX (305) 443-7404